Salvador-Llàcer, P.; Valls Coquillat, J.; Canet Subiela, MJ.; Almenar Terre, V.; Corral, JL. (2022). On the Performance and Power Consumption of Bias-T Based Drivers for High Speed VLC. Journal of Lightwave Technology. 40(18):6078-6086. https://doi.org/10.1109/JLT.2022.3190936

# On the Performance and Power Consumption of Bias-T Based Drivers for High Speed VLC

Pau Salvador, Javier Valls, Maria Jose Canet, Vicenç Almenar, Juan Luis Corral, *Senior Member, IEEE*

***Abstract*—LED lamps have become the predominant technology for lighting thanks to their low power consumption. Recently, the joint use of these devices for lighting and data transmission has aroused interest in the research community as a future green communication technology. During this time, many of the advances developed in this area have been demonstrated with experimental setups using LED drivers based on bias-T, thanks to their ease to combine signal modulation and LED bias. This article discusses the impact of the output impedance of the bias-T driver and the driver-LED connection parasitics on the performance and energy efficiency of the VLC system. It is concluded that the output impedance of the driver not only affects energy efficiency but also modifies the frequency response and, therefore, the LED's capacity to be modulated. A low output impedance driver is shown to offer a substantial improvement in the energy efficiency of the VLC driver.**

***Index Terms*—White LED, energy efficiency, consumption factor, VLC.**

## I. Introduction

VISIBLE Light Communications (VLC) are gaining research interest in recent years as an energy-efficient wireless communication technology for indoor environments, thanks to the growing use of LEDs for lighting and their shared utilization for data transmission [1], [2], via intensity modulation.

In [3] the consumption factor theory was stated as a method to analyze and compare, from the energy efficiency point of view, design choices for wireless communications systems. It makes use of the consumption factor (CF) parameter, which is defined as the ratio between the transmitted data rate and the power consumed in the context of communications systems, and it is usually given in bits per Joule. The higher the CF, the less the energy per transmitted bit spent by a communication system. In order to evaluate each component of the system included in the signal path, in [3] the efficiency of a component was defined as the ratio between the signal power delivered to the next stage and the total power used by the component, including the power not delivered as signal power.

This work was supported in part by MCIN/AEI/10.13039/501100011033 and in part by the European Union (ERDF A way of making Europe) under Grants RTI2018-101658-B100 and RTI2018-101296-B-I00, and in part by Ministerio de Ciencia, Innovación y Universidades para la Formación de Profesorado Universitario under Grant FPU19/04648 (Corresponding author: Pau Salvador)

P. Salvador, J. Valls, M.J. Canet, and V. Almenar are with the Instituto de Telecomunicaciones y Aplicaciones Multimedia, Universitat Politècnica de València, Valencia 46730, Spain (e-mail: pasallla@upv.es; jvalls@upv.es; macasu@upv.es; valmenar@upv.es).

J.L. Corral is with the Instituto Universitario de Tecnología Nanofotónica, Universitat Politècnica de València, Valencia 46730, Spain (e-mail:jlcorral@upv.es).

A very important conclusion from [3] is that the efficiency of the stage that handles the highest level of signal power is the one that has a greater effect on the consumption factor of the whole system. Therefore, its efficiency must be maximized to maximize the CF of the system. In the context of VLC, this conclusion clearly puts the focus on the LED driver, which is the component that handles the highest signal levels.

In recent years, many LED drivers have been proposed [4]. They can be divided into two categories depending on how they implement the modulation: linear model modulation (LMM) or switching mode modulation (SMM). LMM drivers use transistors operating in their linear region, so they are always dissipating because they require additional power to maintain the operating point of the transistors. SMM drivers use transistors that switch between cutoff and saturation regions, and the square waveform they generate is then filtered with an LC bandpass or lowpass filter. The power efficiency, measured as the ratio of the average output power to the input power of the entire driver, is higher for the SMM than for the LMM, since in SMM drivers the conduction and switching losses are low, while LMM always requires additional power for biasing. Due to their high efficiency, SMM are commonly used to implement LED illumination drivers. However, when used for VLC, LMM-based drivers achieve higher data rates due to their wider modulation bandwidth and the ability to use more spectrally efficient modulation schemes, although with lower power efficiency [4].

On the other hand, the consumption factor theory of [3] was applied in [5] to analyze the energy efficiency of a complete Li-Fi VLC link, which includes the modulation schemes, the type of driver, the LED and channel propagation models, the light sensor and the low noise amplifier. The authors conclude that for high data rate VLC systems, LMM drivers are more efficient in terms of CF than SMM, because they require less energy per transmitted bit, and the CF achieved with SMM drivers drops severely with the signal bandwidth.

There are two main topologies of LMM drivers [6]: bias-T based and serial transistor based (also known as serial-F, as it is usually implemented with FET transistors). In the bias-T approach, the bias current and the amplified modulation signal are decoupled by the bias-T circuit. However, in the series transistor approach, bias current and modulation are not decoupled, but are provided both by the transistor. Between these two options, the bias-T based driver is the most popular one due to its simplicity to be implemented, and many of the advances in VLC research published in the literature are based on experiments carried out with this type of driver ([7], [8], [9], [10], [11], [12], [13], [14], [15], [16]) or the direct

use of an arbitrary wave generator and a bias-T ([17], [18], [19], [20], [21], [22]). In these experiments, it has not been taken into account that the dynamic resistance of the LED is very small, in the order of ohms, and, therefore, it is very unbalanced with respect to the conventional 50 Ω impedance used to drive the LEDs.

Although different researchers have pointed out the problem of driving LEDs, which have low input impedance, with bias-T drivers [23], [24], [25], to the best of the authors' knowledge, its impact on frequency response, performance and power consumption has not been evaluated yet. In this paper we analyze this impact. Two drivers with output impedance of 0 Ω and 50 Ω were used to modulate different LEDs and to measure their frequency response. Additionally, the throughput of an OFDM transmission was measured and the power consumption of the drivers were calculated to estimate their consumption factor.

The paper is organized as follows. Section II introduces the small-signal circuital model of the driver and LED and the power and efficiency equations used in the paper; Section III presents a low output impedance bias-T based driver; Section IV describes the experimental setup and the procedure to perform the different measurements; Section V presents and analyzes the results; finally, Section VI summarizes the conclusions.

## II. Blue LED circuital models

Several small-signal circuital models of LEDs for VLC can be found in the literature ([26], [27], [7], [28]). These proposals include the electrical parasitics due to bonding and packaging in lighting fixtures, which cause LEDs not to behave as $1^{st}$-order systems.

On the other hand, [29] proposes a linear system model for the white LED, which separates the effect of the blue LED (electrical domain) and that of the phosphor coating (optical domain). Taking into account the parasitics, the blue LED is modelled as a $2^{nd}$-order system, and the presented measurements corroborate its validity. In this section, we will focus on the blue LED because power transfer from driver to LED takes place exclusively in the electrical domain. As in [29], the LED circuital model of [7] with the formulation of [26], [27] is used to show not only the effect of the driver output resistance and the parasitics on the LED frequency response, but also the effect on the energy efficiency.

Fig. 1 represents the $2^n$-order circuital model of an LED. It includes the output stage of the driver (a voltage source $v_s$ with its output resistance $R_g$), the equivalent model of the intrinsic LED (its dynamic resistance $r_d$ and its junction capacitance $C_d$) and the parasitic inductance $L_s$ and resistance $R_s$ due to the LED package and the lighting fixture. $v_{PD}$ is the voltage at the photodetector output, which is proportional to the current in the LED intrinsic resistance, $i_d$. The gain coefficient $h$ includes the effect of LED efficiency, channel attenuation, photodetector responsivity and gain of the transimpedance amplifier [29].

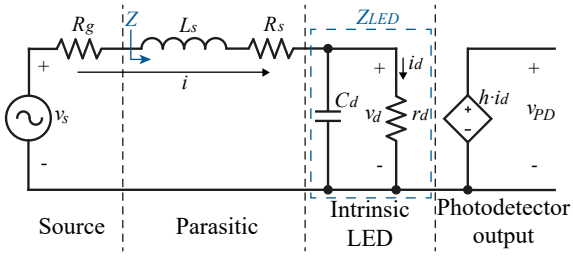


Fig. 1. Circuital LED model including parasitic components

### A. Effect of the driver output resistance on the frequency response

Eq. 1 shows the transfer function $H_L(s)=\frac{V_{PD}(s)}{V_s(s)}$ of the LED circuital model in Fig. 1, where $Z_s=j\omega L_s+R_s$ is the serial parasitic impedance and $Z_{LED}=r_d//\frac{1}{j\omega C_d}$ is the impedance of the intrinsic LED. Its poles are formulated in Eq. 2. Note that the driver output resistance, $R_g$, modifies the position of the poles and thus the frequency response of the system. The influence of $R_g$ depends on the specific values of the intrinsic LED and parasitic components, as will be shown in Section V for two different LEDs.

$$H_L(s)=\frac{V_{PD}(s)}{V_s(s)} = \frac{Z_{LED}}{(R_g+Z_s+Z_{LED})}\cdot\frac{h}{r_d} = \\ =\frac{h}{r_dC_dL_ss^2+\left((R_g+R_s)r_dC_d+L_s\right)s+(R_g+R_s+r_d)} \quad (1)$$

$$s_{1,2}=-\left(\frac{R_g+R_s}{2L_s}+\frac{1}{2r_dC_d}\right)\pm\sqrt{\left(\frac{R_g+R_s}{2L_s}-\frac{1}{2r_dC_d}\right)^2-\frac{1}{C_dL_s}} \quad (2)$$

### B. Effect of the driver output resistance on the energy efficiency

An energy efficiency and power consumption analysis of LEDs for VLC based on a $2^n$-order circuital model was presented in [28]; however, it did not consider the driver output resistance $R_g$. Here we present an expression for LED energy efficiency including the effect of $R_g$.

Taking the voltage $v_s$ in Fig. 1 as the complex effective amplitude or phasor of a signal at an angular frequency $\omega$, the active power, $P_{GEN}(\omega)$, delivered by that voltage source can be obtained as:

$$P_{GEN}(\omega) = \mathrm{Re}\{v_s\cdot i^*\} = |v_s|^2\cdot\mathrm{Re}\left\{\frac{1}{R_g+Z}\right\}, \quad (3)$$

where $Z=Z_s+Z_{LED}$ is the impedance seen by the driver (voltage source) and includes the parasitic components and the intrinsic LED, $i^*$ is the complex conjugated value of the effective current provided by the source $v_s$ and Re{} takes the real part. It is important to point out that according to (Eq. 3) different voltage amplitudes would be required at the source in order to deliver the same power when drivers with different output resistance were compared.

Next, the active power consumed by the LED ($P_{LED}(\omega)$) can be obtained as:

$$P_{LED}(\omega) = \mathrm{Re}\{v_d \cdot i_d^*\} = \frac{|v_d|^2}{r_d} = \frac{|v_s|^2}{r_d} \cdot \left|\frac{Z_{LED}}{R_g+Z}\right|^2, \quad (4)$$

where $v_d$ is the voltage in $r_d$ and $i_d{}^*$ is the complex conjugated value of the current on $r_d$.

Finally, we define the system efficiency, $\xi(\omega)$, as the ratio between the voltage source and LED active powers (Eq. 5).

$$\xi(\omega) = \frac{P_{LED}(\omega)}{P_{GEN}(\omega)} = \frac{r_d}{\left(1+\omega^2 C_d^2 r_d^2\right) \cdot (R_g + R_s) + r_d} \quad (5)$$

### C. Effect of the electrical parasitics on the energy efficiency and the frequency response

It is interesting to note that the efficiency expression defined in Eq. 5 does not depend on the parasitic series inductance, $L_s$. As expected, the power efficiency depends on the relationship between the dynamic resistance of the LED, $r_d$, and all the resistances included in the circuital model shown in Fig. 1. The power efficiency also depends on the LED junction capacitance, $C_d$, so the efficiency decreases as the frequency increases. Although the series inductance $L_s$ does not play any role in the energy efficiency of the VLC driver, it undoubtedly affects the current, $i$, generated by the voltage source. As both powers $P_{GEN}$ and $P_{LED}$ are proportional to $|i|^2$ ($|i_d|^2$ being proportional to $|i|^2$), these dependencies cancel each other out when obtaining the efficiency according to Eq. 5.

On the other side, Eq. 1 and Eq. 2 shows that $L_s$ greatly affects the frequency response of the LED. At high frequency, $Z_s$ increases due to the $j\omega L_s$ term and therefore $v_d$ (as the voltage divider between $Z_s$ and $Z_{LED}$) decreases, as it does $i_d$ and the emitted optical power. Therefore, for high-speed VLC, it is really important to take great care of the integration of the driver and the LED in the lighting fixture in order to keep the parasitic inductance as small as possible.

### D. Response and efficiency in the flat region

We can use Eq. 5 to assess the power efficiency of any specific LED once the components of the circuit model in Fig. 1 are estimated. As an example, Fig. 2 shows the calculated power efficiency for the LEDs used in Section IV (LED1: $R_s = 0.92\,\Omega$, $r_d = 4.35\,\Omega$, $C_d = 3.2\,nF$; LED2: $R_s = 0.7\,\Omega$, $r_d = 2.36\,\Omega$, $C_d = 3\,nF$) when the output resistance of the driver is selected as $R_g = 0\,\Omega$ or $R_g = 50\,\Omega$. The power efficiency of the system is strongly affected by the selection of the output resistance of the voltage driver. For these LEDs, the power efficiency at low frequencies changes from 0.82 and 0.77 when $R_g = 0\,\Omega$ to 0.08 and 0.04 for the $R_g = 50\,\Omega$ case.

At low frequencies, the power efficiency in Fig. 2 and the frequency response are shown to be constant, corresponding to a circuit model without any reactive component. For this frequency range, Fig. 3 shows the simplified LED circuital model and Eq. 6 its gain.

$$\frac{v_{PD}(t)}{v_s(t)} = \frac{h}{R_g + R_s + r_d} \quad (6)$$

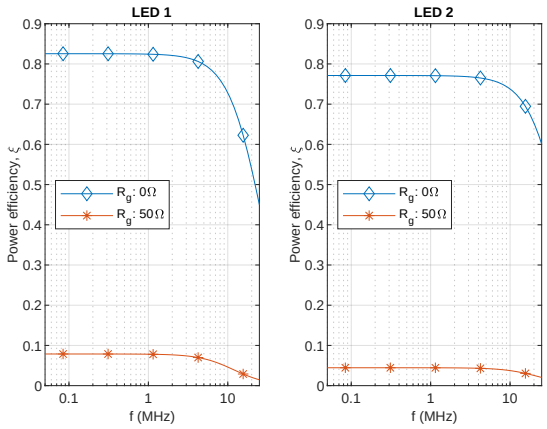


Fig. 2. Estimated power efficiency as a function of frequency for two different values of driver output resistance ($R_g = 50\,\Omega$ and $R_g = 0\,\Omega$).

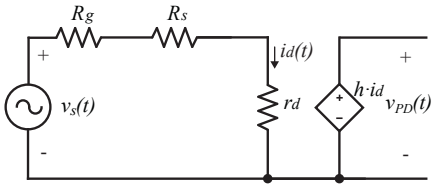


Fig. 3. LED Model in the flat region of its frequency response

Without loss of generality, we will express the signal generated by the voltage source as $v_s(t) = v_s \cdot m(t)$ where $v_s$ is the peak amplitude of $v_s(t)$, and $m(t)$ is a normalized modulating signal ($max(|m(t)|) = 1$) with root mean square (RMS) value $\alpha_m$ ($\alpha_m^2 = \overline{m^2(t)}$). Accordingly, the photodetected voltage can be expressed as $v_{PD}(t) = v_{PD} \cdot m(t)$.

Based on this simplified model, the active power delivered by the voltage source ($P_{GEN}$), the active power consumed by the LED ($P_{LED}$) and the efficiency ($\xi$) for the flat region can be rewritten as shown in Eq. 7, Eq. 8 and Eq. 9, respectively. These equations can also be obtained from Eq. 3, Eq. 4 and Eq. 5 when approached at low frequency.

$$P_{GEN} = \frac{\overline{v_s^2(t)}}{R_g + R_s + r_d} = \frac{v_s^2 \cdot \alpha_m^2}{R_g + R_s + r_d} \quad (7)$$

$$P_{LED} = \frac{\overline{v_s^2(t)} \cdot r_d}{(R_g + R_s + r_d)^2} = \frac{v_s^2 \cdot \alpha_m^2 \cdot r_d}{(R_g + R_s + r_d)^2} \quad (8)$$

$$\xi = \frac{P_{LED}}{P_{GEN}} = \frac{r_d}{R_g + R_s + r_d} \quad (9)$$

The power efficiency of the LED driver is shown to be compromised by the voltage source output impedance, $R_g$, and the parasitic resistance of the LED package and the driver-LED interconnection in the lighting fixture, $R_s$. The optimum design in terms of power efficiency will require a driver with low output resistance and a short driver-LED connection.

We define the constant $k$ as the ratio between the efficiency of the driver with output resistance $R_g = 0\,\Omega$ ($\xi_0$) and the

efficiency of the driver with $R_g = 50\,\Omega$ ($\xi_{50}$) in Eq. 10. Given that $k > 1$, $\xi_0$ is always $k$ times higher than $\xi_{50}$.

$$k = \frac{\xi_0}{\xi_{50}} = \frac{50+R_s+r_d}{R_s+r_d} \tag{10}$$

Note that it can be concluded from Eq. 6 and Eq. 10 that a driver with output resistance $R_g = 50\ \Omega$ requires the source signal amplitude ($v_s$) to be $k$ times higher than the source of a driver with output resistance $R_g = 0\,\Omega$ in order to produce the same voltage at the photodetector output, $v_{PD}$.

For their use in the following sections, the previously defined variables are renamed with suffixes 0 or 50, indicating if they are obtained with $0\,\Omega$ or $50\,\Omega$ drivers, *e.g.* $P_{LED0}$, $P_{GEN0}$ and $v_{s0}$ are the power consumption of the LED, the signal power supplied by the driver and the source voltage amplitude, respectively, with the $R_g = 0\,\Omega$ driver.

## III. Low output impedance LED driver

The operational amplifier OPA2677 was selected to implement a very low output impedance driver due to several facts: $1^{st}$) it has a very low output impedance in the whole range of interest (lower than 0.1 Ω up to 10 MHz and close to 1 Ω at 30 MHz); $2^{nd}$) it has a high output current of 500 mA, which is enough to drive the tested LEDs; and $3^{rd}$) it has a wide bandwidth that provides a flat response in the frequencies of interest. The circuital scheme of the driver and its frequency response are shown in Fig. 4. It uses a non-inverting voltage amplification configuration that provides a gain of 9.5 dB. Its small-signal input impedance is fixed to 50 Ω to match the impedance of the arbitrary wave generator, and a bias network is included to avoid symmetric voltage supply.

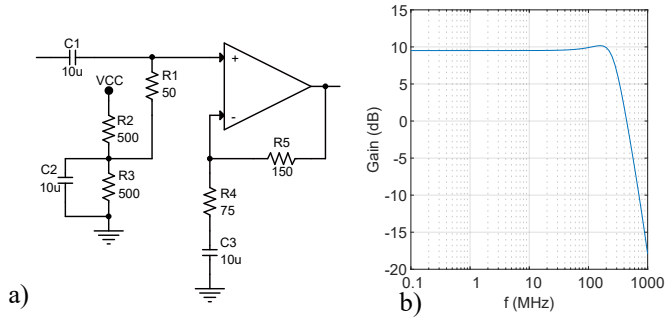


Fig. 4. LED driver a) circuital scheme; b) frequency response.

## IV. Experimental setup

Fig. 5 shows the scheme of the experimental VLC setup used to measure the impact of the driver output resistance on the LED frequency response and its power transfer efficiency, and its implementation is shown in Fig. 6. At the transmitter, an OFDM signal was generated by an arbitrary wave generator (AWG) Siglent SDG6022X, then it was amplified by the OPA2677-based driver (DRIVER) and it passed through a bias-T with a capacity of 22 µF and an inductance of 1 mH, which was connected to the LED under test with a reflector C16902_ALISE-110-WW. We also designed a driver with $R_g = 50\,\Omega$ for the test using the same circuit in Fig. 4 and adding a $50\,\Omega$ resistance at the OPA2677 output. The receiver was composed of the lens ACL25416U-A used with the PDA10A amplified photodetector, which was connected to an oscilloscope Rohde&Schwarz RTM3004.

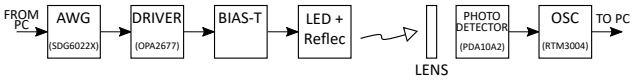


Fig. 5. Scheme of the experimental VLC setup.

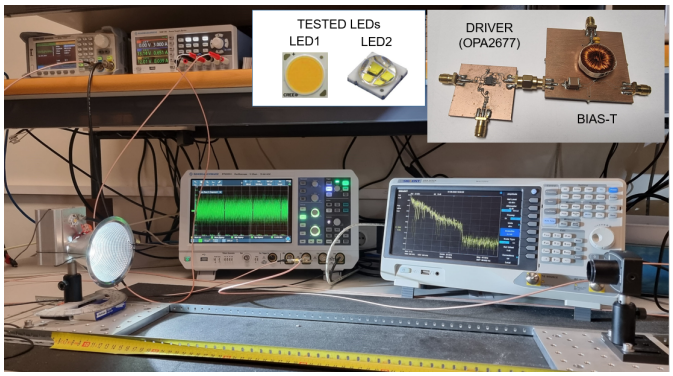


Fig. 6. Implemented experimental VLC setup.

Two different high luminous flux white LEDs were used in the experiments: CXB1830-0000-000N0BV265E from Cree (LED1), which is a COB (chip-on-board) diode type; and LZ4-40CW08-0065 from OSRAM (LED2), which is composed of 4 LEDs connected in series. Table I summarizes their main characteristics and includes the bias current used in the experiments. The DC-biased OFDM [30] was configured as detailed in Table II. In this setup we used a DC-biased OFDM with a RMS modulation index of $\alpha_m = 0.23$, so significant non-linear distortions were avoided [6].

TABLE I
LEDs features and $I_{bias}$

| Feature | LED1 | LED2 |
|---|---|---|
| Correlated Color Temperature | 6500 | 6500 |
| Forward Voltage (V) | 35 | 12.6 |
| DC Forward Current (mA) | 800 | 700 |
| Luminous Flux (lm) | 4600 | 800 |
| Viewing angle (deg.) | 115 | 90 |
| $I_{bias}$ (mA) | 600 | 650 |

TABLE II
OFDM transmission parameters

| | |
|---|---|
| QAM order | 4 - 1024 |
| FFT length | 256 |
| Inactive high frequency subcarriers | 64 |
| Sampling frequency | 100 MHz |
| Bandwidth (BW) | 25 MHz |

In order to compare the frequency response of each LED with $R_g = 0\,\Omega$ and $R_g = 50\,\Omega$ drivers and to study the effect of

$R_g$ on the throughput and on the CF as a function of the distance between the LED and the photodetector, two experiments were carried out. Firstly, the throughput and CF for different distances were measured for the same power supplied by the source to check the effect of the driver output impedance. Secondly, the throughput and CF were obtained for the same LED power consumption. In this case, the two versions of the driver generated different powers to compensate for the influence of the different output impedances. This measurement was used to check the effect of the different frequency responses on throughput and CF. Next, the procedure followed to perform both experiments is described. For the sake of simplicity, although the OFDM signals are transmitted beyond the −3 dB LED bandwidth, we perform the calculations in the region where the LED frequency response is flat, using the circuit model of Fig. 3 and the equations of Section II-D. The resistive component values, $r_d$ and $R_s$, and the values of $\xi$ and $k$ are shown in Table III for LED1 and LED2. $r_d$ was estimated from the slope of the LEDs I/V curve at the bias point, $R_s$ using Eq. 10 once $k$ was obtained as explained in Section IV-B, and $\xi$ was obtained using Eq. 9.

TABLE III
LEDs RESISTIVE COMPONENTS, $k$ AND $\xi$ VALUES

| Feature | LED1 | LED2 |
|---|---|---|
| $r_d\,(\Omega)$ | 4.35 | 2.36 |
| $R_s\,(\Omega)$ | 0.92 | 0.7 |
| $k$ | 10.48 | 17.32 |
| $\xi_0$ | 0.82 | 0.77 |
| $\xi_{50}$ | 0.08 | 0.04 |

### A. Measurements with the same power supplied by the source

When the same power is supplied by the source, the photodetector receives less signal amplitude with the $R_g = 50\,\Omega$ driver than with the $R_g = 0\,\Omega$ driver due to the power wasted in the driver output resistance. In this case, if we force $P_{GEN0} = P_{GEN50}$, as $P_{GEN0} = P_{LED0}/\xi_0$ and $P_{GEN50} = P_{LED50}/\xi_{50}$ (Eq. 9), then $P_{LED0} = k \cdot P_{LED50}$ (Eq. 10), so the $R_g = 0\,\Omega$ driver transfers a $k$ times higher power to the LED. In addition, from Eq. 7, it can be deduced that $v_{s50} = \sqrt{k} \cdot v_{s0}$ (the details of these calculus are in Appendix A). Therefore, to perform this experiment the amplitude of the source with the $R_g = 50\,\Omega$ driver must be forced to be $\sqrt{k}$ times higher than the one with the $R_g = 0\,\Omega$ driver.

According to Eq. 6 the relation between photodetected voltages will be $v_{PD0} = \sqrt{k} \cdot v_{PD50}$ when $v_{s50} = \sqrt{k} \cdot v_{s0}$. Consequently, we can verify that both drivers are configured correctly as $P_{GEN0} = P_{GEN50}$ if, when measuring the output of the photodetector, a voltage value $\sqrt{k}$ higher is obtained with the $R_g = 0\,\Omega$ driver.

### B. Measurements with the same LED power consumption

As explained in Section II-D, the configuration with the $R_g = 50\,\Omega$ driver requires a greater source amplitude to generate the same voltage at the photodiode as the $R_g = 0\,\Omega$ driver or, in other words, to have the same power consumption at the LED. Clearly, this is caused by driving the low resistance of the LED ($R_s + r_d$), which is a few ohms, with a driver whose output impedance is $50\,\Omega$.

If we want the LED to have the same power consumption with both drivers ($P_{LED0} = P_{LED50}$), as $P_{LED0} = \xi_0 \cdot P_{GEN0}$ and $P_{LED50} = \xi_{50} \cdot P_{GEN50}$ (Eq. 9), then $P_{GEN50} = k \cdot P_{GEN0}$ (Eq. 10), so the $R_g = 50\,\Omega$ driver has to supply a power $k$ times higher. In addition, it can be deduced from Eq. 8 that $v_{s50} = k \cdot v_{s0}$ (the details of these calculus are in Appendix B) and $v_{PD50} = v_{PD0}$ from Eq. 6. Therefore, to perform this experiment the amplitude of the source with the $R_g = 50\,\Omega$ driver must be forced to be $k$ times higher than the one with the $R_g = 0\,\Omega$ driver. The value of $k$ in the flat region was obtained experimentally by $1^{st}$) measuring $v_{PD0}$ with $R_g = 0\,\Omega$ for a given $v_{s0}$ and $2^{nd}$) increasing the $v_{s50}$ with $R_g = 50\,\Omega$ up to measure $v_{PD50} = v_{PD0}$, so in this case $k = \frac{v_{s50}}{v_{s0}}$.

## V. RESULTS

This section presents the results of measurements performed using the experimental setup described in the previous section. The frequency response, the throughput and CF results obtained for the same LED power consumption or the same power supply are analyzed. Additionally, an study about how to reach the highest data rate with the highest efficiency is presented.

Although Section II was focused on the blue LED small-signal circuital model (which is the one that has influence on the power consumption), here we present real measurements for white LEDs. This kind of LEDs generates blue light (circuit model in Fig. 1) and yellow light, which comes from the phosphor coating effect that adds a pole and a zero to the frequency response of the blue LED [29]. However, since our power consumption and efficiency calculations are done in the flat region, the equations in Section II-D are valid, with the exception of $h$ in Eq. 6, whose value is different for the white LED.

The frequency response of a VLC channel is low-pass, as can be seen in the measurements shown in Fig. 7. If high throughput is required, the LED channel must be used far beyond the 3 dB frequency bandwidth. As OFDM can be configured to transport different QAM modulation orders, the selection of the number of bits in each subcarrier can be optimized according to the attenuation of the channel in order to maximize the bit rate. This strategy is called adaptive bit loading and has been thoroughly used in the VLC literature [11], [31] and examples therein. A simple and efficient solution is based on a look-up table of predefined signal-to-noise ratio (SNR) threshold values that are employed to select the number of bits transmitted in each subcarrier [32]. To set the threshold values we took into account the SNR that gives a BER under $3.8{\times}10^{-3}$, which allows error free transmission if forward error correction (FEC) with hard detection (HD) is employed [33] (also known as HD-FEC threshold in the literature). To this end, the next procedure was carried out in all the experiments presented in this section: 1) OFDM with 4-QAM in all subcarriers was transmitted; 2) the Error Vector

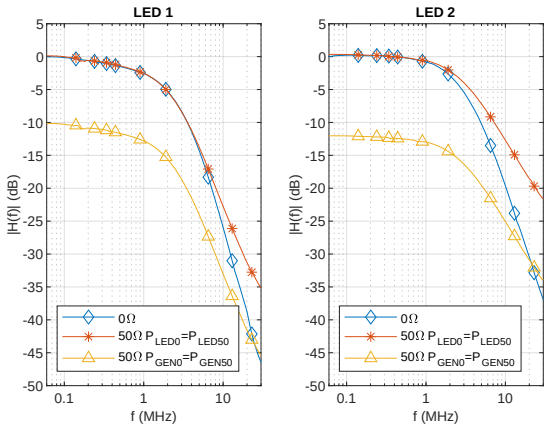


Fig. 7. LED1 and LED2 frequency response. The 50 Ω curves are plotted normalized with respect to the 0 Ω curve

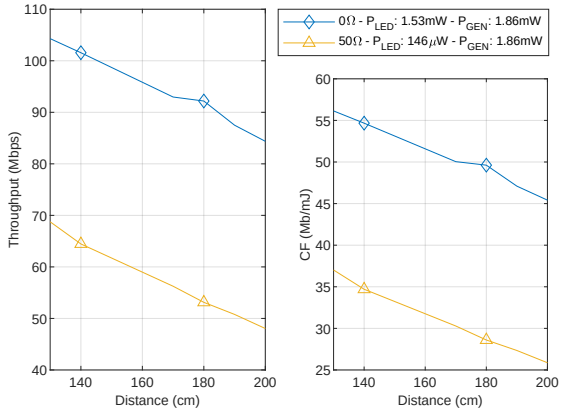


Fig. 8. Throughput and CF measurements of LED1 with the same power generated in the driver ($P_{GEN0}$= $P_{GEN50}$ = 1.86 mW)

Magnitude (EVM) was measured for each subcarrier [34]; 3) the SNR was estimated making use of the EVM; 4) the QAM order was selected according to the threshold look-up-table. The final throughput is obtained aggregating the number of bits transmitted by all the subcarriers. On the other hand, CF is obtained as Eq. 11, where $P_{GEN}$ is calculated with Eq. 7.

$$CF = \frac{Throughput}{P_{GEN}} \tag{11}$$

### A. Measurements with the same power supplied by the source

This section shows the results obtained when the same power supply was generated for both drivers using the procedure explained in Section IV-A. Fig. 7 shows the measured frequency responses of white LED1 and LED2 obtained with both drivers. The curve for the $R_g = 50\,\Omega$ driver when the source generates the same power ($P_{GEN0} = P_{GEN50}$) has lower gain than the one for $R_g = 0\,\Omega$ and is plotted normalized with respect to it. At low frequency (flat response), the difference between $R_g = 50\,\Omega$ and $R_g = 0\,\Omega$ curves is 10.27 dB and 12.37 dB for LED1 and LED2, respectively, which approximately corresponds to the theoretical value $20\log_{10}(\sqrt{k})$ (10.20 dB and 12.37 dB).

Fig. 8 and Fig. 9 show the throughput and the CF as a function of the LED-photodetector distance for LED1 and LED2, respectively. In both figures, $P_{GEN0} = P_{GEN50}$ (1.86 mW for LED1 and 1.17 mW for LED2) and $P_{LED0} = k \cdot P_{LED50}$, so $P_{LED}$ is $k$ times lower for the $R_g = 50\,\Omega$ driver ($k = 10.48$ for LED1: 146 $\mu$W versus 1.53 mW; and $k = 17.32$ for LED2: 902 $\mu$W versus 52 $\mu$W). As expected, both the throughput and the CF are higher for the $R_g = 0\,\Omega$ driver when the same supply power is used. The difference between the output resistance of the driver and the input resistance of the LED makes the $R_g = 50\,\Omega$ driver to be very energy-inefficient. In this case, the $R_g = 0\,\Omega$ driver is 51.7 % and 75.8 % faster, and 1.5 and 1.8 times more efficient at a distance of 130 cm for LED1 and LED2, respectively, and 75.6 % and 154.2 % faster, and 1.8 and 2.5 times more efficient at a distance of 200 cm for LED1 and LED2, respectively. These improvements increase with the distance of the optical link because the received optical power

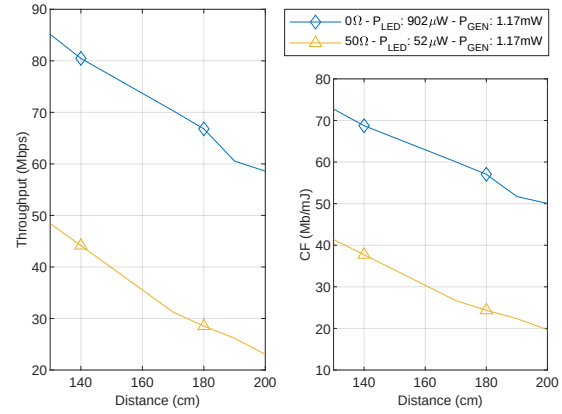


Fig. 9. Throughput and CF measurements of LED2 with the same power generated in the driver ($P_{GEN0}$= $P_{GEN50}$ = 1.17 mW)

is reduced and high-frequency OFDM subcarriers cannot be employed due to the LED frequency response attenuation.

### B. Measurements with the same LED power consumption

The frequency responses of both LEDs are shown in Fig. 7. The curve for the $R_g = 50\,\Omega$ driver has the same gain in the flat region as the one for $R_g = 0\,\Omega$ when $P_{LED0} = P_{LED50}$, and they were plotted normalized with respect to that gain.

The same conclusion as the one extracted from studying the LED circuital model of Fig. 1 is derived: the output resistance of the driver affects the LED frequency response and efficiency. As LED1 and LED2 have different resistive components (see Table III), the impact of $R_g$ on the frequency response is not the same. The cutoff frequency at $-3$ dB of LED1 does not change with $R_g$, it is in both cases $f_{-3dB} = 1.2$ MHz. However, the slope at high frequencies is lower with $R_g = 50\,\Omega$ than with $R_g = 0\,\Omega$. For LED2, selecting $R_g = 50\,\Omega$ changes not only the slope of the frequency response, but also the cutoff frequency, which increases from $f_{-3dB} = 2$ MHz with $R_g = 0\,\Omega$ to $f_{-3dB} = 2.5$ MHz.

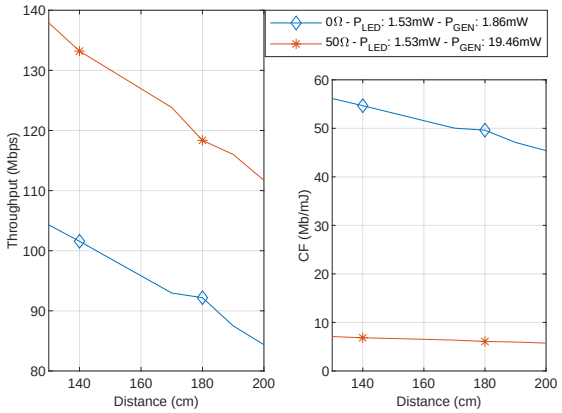


Fig. 10. Throughput and CF measurements of LED1 with the same power consumption in the LED ($P_{LED0} = P_{LED50} = 1.53\,\text{mW}$)

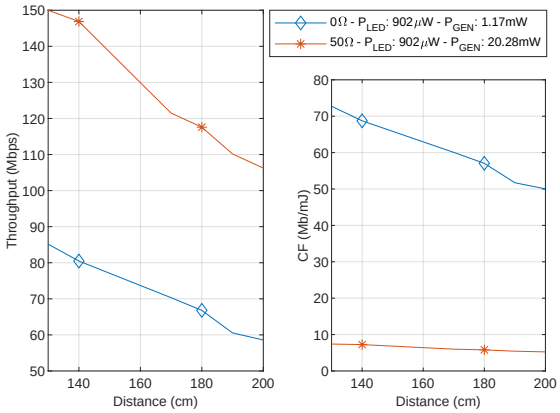


Fig. 11. Throughput and CF measurements of LED2 with the same power consumption in the LED ($P_{LED0} = P_{LED50} = 0.9\,\text{mW}$)

Fig. 10 and Fig. 11 show the throughput (left) and the CF (right) as a function of the LED-photodetector distance for LED1 and LED2, respectively, when the LED power consumption is the same for both drivers. The measurements were done following the procedure explained in Section IV-B. In both figures, $P_{LED0} = P_{LED50}$ (1.53 mW for LED1 and 902 $\mu$W for LED2) and $P_{GEN50} = k \cdot P_{GEN0}$ ($k = 10.48$ for LED1: 19.46 mW versus 1.86 mW; and $k = 17.32$ for LED2: 20.28 mW versus 1.17 mW). This configuration implies that the $R_g = 50\,\Omega$ driver requires $k$ times more power supply to produce the same signal level at the photodetector output as the $R_g = 0\,\Omega$ driver.

As can be seen, the $R_g = 50\,\Omega$ driver achieves higher throughput than the $R_g = 0\,\Omega$ driver for both LEDs. This is due to the influence of $R_g$ on the frequency response: it reduces the attenuation at high frequencies for both LEDs when the drivers have $R_g = 50\,\Omega$. As the transmitted bandwidth (25 MHz) exceeds the $-3$ dB bandwidth of the LEDs, it is possible to charge with higher QAM order the OFDM subcarriers at high frequency. The comparison between frequency responses of Fig. 7 evidences this scenario. The attenuation differences between both frequency response curves at 25 MHz are about 10 dB and 14 dB for LED1 and LED2, respectively. Fig. 12 shows the employed bit loading per OFDM subcarriers for a transmission distance of 130 cm. At this distance, LED1 achieves 137.9 Mbps with 7.1 Mb/mJ and 104.3 Mbps with 56.1 Mb/mJ for $R_g = 50\,\Omega$ and $R_g = 0\,\Omega$ drivers, respectively, *i.e.* the $R_g = 50\,\Omega$ driver is about 32.2 % faster but the $R_g = 0\,\Omega$ driver is 7.9 times more efficient in terms of CF. At the same distance with LED2, the $R_g = 50\,\Omega$ driver is 76.1 % faster but the $R_g = 0\,\Omega$ driver is 9.8 times more efficient. In this case the throughput increment is higher than with LED1 because for LED2 the frequency response with the $R_g = 50\,\Omega$ driver improves much more than with the other LED. At a distance of 200 cm, the $R_g = 50\,\Omega$ driver is 32.4 % and 81.3 % faster, but the $R_g = 0\,\Omega$ driver is 7.9 and 9.6 times more efficient for LED1 and LED2, respectively.

### C. High-throughput configuration

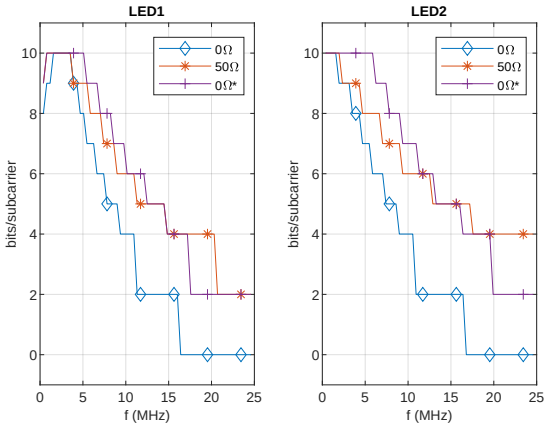


Fig. 12. Bit loading per OFDM subcarrier. $0\,\Omega$ and $50\,\Omega$ curves are obtained generating the same power consumption in the LED ($P_{LED0} = P_{LED50}$) at a distance of 130 cm. Case $0\,\Omega^*$ improves the throughput making use of a higher $P_{GEN}$.

As seen in Section V-B, both LEDs under test achieve higher throughput with the $R_g = 50\,\Omega$ driver if the source amplitude is increased till having the same LED power consumption as with the $R_g = 0\,\Omega$ driver, this is, a $k$ times increase. This throughput improvement is reached at the expense of making the system very inefficient in terms of power consumption (the CF is about 7.9 and 9.8 times lower with the $R_g = 50\,\Omega$ driver for LED1 and LED2, respectively). However, the $R_g = 0\,\Omega$ driver can reach the same throughput if $P_{GEN}$ is increased. A comparison of these results is shown in Table IV where, for each LED, the first line of both $R_g$ shows the results obtained in previous section for a distance of 130 cm. For $R_g = 0\,\Omega$, the line labeled $0^*$ shows how this driver can achieve the same high throughput as the $R_g = 50\,\Omega$ driver (about 138 Mbps and 150 Mbps for LED 1 and LED 2, respectively) if the power supplied by the source ($P_{GEN}$) is increased, but at the expense of a worse CF: now this driver is 1.92 and 1.51 times more efficient than the $R_g = 50\,\Omega$ one in terms of CF for LED1 and LED2, respectively. For this case, Fig. 12 shows the bit loading

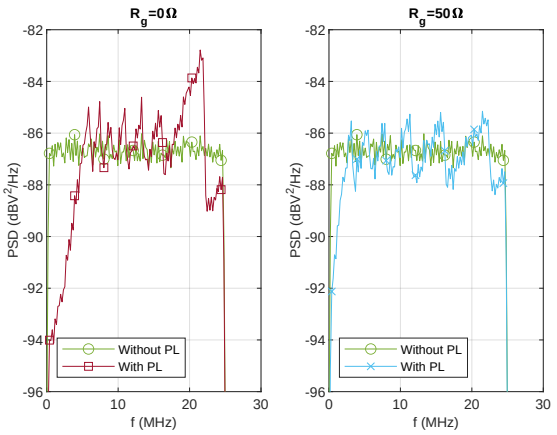


Fig. 13. Transmission spectrum of the normalized modulating signal $m(t)$ with and without power loading (PL) for LED2.

results compared to previous configurations, it can be seen how driver with 0 Ω tends to work better at lower frequencies and driver with 50 Ω can make use of higher order QAM symbols at high frequencies thanks to its better frequency response.

Due to the low-pass characteristic of the LED channel, a known solution to improve the throughput and maintain the power efficiency is to use power loading with a waterfilling strategy [11]. The iterative Hughes-Hartogs algorithm [35] that approaches waterfilling in a practical implementation was developed and tested. The transmitted power spectra for LED2 are shown in Fig. 13 for both $R_g$ and compared with the spectra without power loading. The obtained results are also presented in Table IV. For both LEDs, the last line of each $R_g$ shows how the throughput increases between 5% and 8% for both drivers with similar energy usage. These low improvements were also pointed out in [31], where several power loading algorithms were compared and it was concluded that given the complexity of a waterfilling solution, adaptive bit loading is a more convenient approach.

TABLE IV
THROUGHPUT RESULTS COMPARISON

| | $R_g$ (Ω) | Throughput (Mbps) | $P_{GEN}$ (mW) | CF (Mb/mJ) |
|---|---|---|---|---|
| LED1 | 0 | 104.3 | 1.86 | 56.1 |
| | 0* | 138.3 | 10.17 | 13.6 |
| | 0* with PL | 147.3 | 10.96 | 13.4 |
| | 50 | 137.9 | 19.47 | 7.1 |
| | 50 with PL | 148.8 | 20.66 | 7.2 |
| LED2 | 0 | 85.2 | 1.17 | 72.8 |
| | 0* | 152 | 13.59 | 11.2 |
| | 0* with PL | 161.3 | 13.84 | 11.7 |
| | 50 | 150 | 20.28 | 7.4 |
| | 50 with PL | 157.4 | 19.36 | 8.1 |

0* means 0Ω with more $P_{GEN}$

## VI. Conclusion

In this paper we have shown, analytically and experimentally, how the output impedance of a bias-T driver influences the energy efficiency of a VLC system and changes its frequency response. Besides, a low output impedance driver has been presented.

Experimental measurements showed that data rate and consumption factor achieved with a driver with a 0 Ω output impedance were about 50% - 150% (depending on the LED and the distance) higher than the ones achieved with the conventional 50 Ω driver when both drivers generate the same signal power. Hence, the use of conventional LED drivers or signal generators, with an output impedance of 50 Ω, causes low energy efficiency and low consumption factor due to the low internal resistance of the LED. The best energy efficiency is obtained with LED drivers with the lowest possible output impedance.

If the comparison is made when a constant power is delivered to the LED, the throughput of the 50 Ω driver was about 30% - 80% higher thanks to a better frequency response of the VLC link. However, this improvement was achieved at the expense of a higher consumption factor: the CF of the 50 Ω driver was shown to be about 8 - 10 times worse. It was also shown that to achieve the same throughput, the 0 Ω driver requires lower power and achieves better CF. We concluded that the results and optimizations of data transmission experiments based on 50 Ω LED drivers are not valid for realistic VLC scenarios where more efficient drivers (with lower output impedance) need to be used.

On the other hand, an analysis of how the parasitic components due to the LED package and the lighting fixture individually affect the frequency response and power efficiency of the LED driver has been also presented. The parasitic resistance has a direct influence on the power efficiency and its value should be kept as low as possible, whereas the parasitic inductance has no influence at all in the power efficiency. However, this inductance has an important effect in the frequency response of the LED, reducing the emitted optical power at high frequency.

Consequently, as future lines of research, it is proposed to work on integrating the low output impedance LED driver and bias-T within the LED lighting fixture, to minimize parasitic effects and maximize the efficiency of the lighting and communication features.

## Appendix A
## Calculus for the same power supplied by the source

On the one hand, using Eq. 7 and $P_{GEN50} = P_{GEN0}$:

$$\frac{v_{s50}^2 \cdot \alpha_m^2}{50 + R_s + r_d} = \frac{v_{s0}^2 \cdot \alpha_m^2}{R_s + r_d} \tag{12}$$

Isolating $v_{s50}$ and using Eq. 10:

$$v_{s50} = \sqrt{\frac{50 + R_s + r_d}{R_s + r_d}} \cdot v_{s0} = \sqrt{k} \cdot v_{s0} \tag{13}$$

On the other hand, using Eq. 9 and $P_{GEN50} = P_{GEN0}$:

$$\frac{P_{LED0}}{\xi_0} = \frac{P_{LED50}}{\xi_{50}} \tag{14}$$

Isolating $P_{LED0}$ and using Eq. 10:

$$P_{LED0} = \frac{\xi_0}{\xi_{50}} \cdot P_{LED50} = k \cdot P_{LED50} \tag{15}$$

## Appendix B
## Calculus for the same LED power consumption

On the one hand, using Eq. 8 and $P_{LED50} = P_{LED0}$:

$$\frac{v_{s50}^2 \cdot \alpha_m^2 \cdot r_d}{(50 + R_s + r_d)^2} = \frac{v_{s0}^2 \cdot \alpha_m^2 \cdot r_d}{(R_s + r_d)^2} \tag{16}$$

Isolating $v_{s50}$ and using Eq. 10:

$$v_{s50} = \frac{50 + R_s + r_d}{R_s + r_d} \cdot v_{s0} = k \cdot v_{s0} \tag{17}$$

On the other hand, using Eq. 9 and $P_{LED50} = P_{LED0}$:

$$P_{GEN0} \cdot \xi_0 = P_{GEN50} \cdot \xi_{50} \tag{18}$$

Isolating $P_{GEN50}$ and using Eq. 10:

$$P_{GEN50} = \frac{\xi_0}{\xi_{50}} \cdot P_{GEN0} = k \cdot P_{GEN0} \tag{19}$$

## References


[1] A. Tsiatmas, C. P. Baggen, F. M. Willems, J.-P. M. Linnartz, and J. W. Bergmans, "An illumination perspective on visible light communications," *IEEE Communications Magazine*, vol. 52, no. 7, pp. 64–71, 2014.

[2] H. Haas, L. Yin, Y. Wang, and C. Chen, "What is LiFi?" *Journal of Lightwave Technology*, vol. 34, no. 6, pp. 1533–1544, 2016.

[3] J. N. Murdock and T. S. Rappaport, "Consumption factor and power-efficiency factor: A theory for evaluating the energy efficiency of cascaded communication systems," *IEEE Journal on Selected Areas in Communications*, vol. 32, no. 2, pp. 221–236, 2014.

[4] L. Teixeira, F. Loose, J. M. Alonso, C. H. Barriquello, V. Alfonso Reguera, and M. A. Dalla Costa, "A review of visible light communication LED drivers," *IEEE Journal of Emerging and Selected Topics in Power Electronics*, vol. 10, no. 1, pp. 919–933, 2022.

[5] L. Teixeira, F. Loose, C. H. Barriquello, V. A. Reguera, M. A. D. Costa, and J. M. Alonso, "On energy efficiency of visible light communication systems," *IEEE Journal of Emerging and Selected Topics in Power Electronics*, vol. 9, no. 5, pp. 6396–6407, 2021.

[6] X. Deng, K. Arulandu, Y. Wu, S. Mardanikorani, G. Zhou, and J.-P. M. G. Linnartz, "Modeling and analysis of transmitter performance in visible light communications," *IEEE Transactions on Vehicular Technology*, vol. 68, no. 3, pp. 2316–2331, 2019.

[7] P.-C. Song, Z.-Y. Wu, X.-D. An, and J. Wang, "Energy efficiency analysis of light-emitting diodes with high modulation bandwidth," *IEEE Electron Device Letters*, vol. 42, no. 7, pp. 1025–1028, 2021.

[8] X. Guo and N. Chi, "Superposed 32QAM constellation design for 2 x 2 spatial multiplexing MIMO VLC systems," *Journal of Lightwave Technology*, vol. 38, no. 7, pp. 1702–1711, 2020.

[9] P. Nabavi and M. Yuksel, "Comprehensive design and prototype of VLC receivers with large detection areas," *Journal of Lightwave Technology*, vol. 38, no. 16, pp. 4187–4204, 2020.

[10] P. Chvojka, A. Burton, P. Pesek, X. Li, Z. Ghassemlooy, S. Zvanovec, and P. A. Haigh, "Visible light communications: increasing data rates with polarization division multiplexing," *Opt. Lett.*, vol. 45, no. 11, pp. 2977–2980, Jun 2020.

[11] S. Mardanikorani, X. Deng, and J.-P. M. G. Linnartz, "Sub-carrier loading strategies for DCO-OFDM LED communication," *IEEE Transactions on Communications*, vol. 68, no. 2, pp. 1101–1117, 2020.

[12] M. Mohammedi Merah, H. Guan, and L. Chassagne, "Experimental multi-user visible light communication attocell using multiband carrierless amplitude and phase modulation," *IEEE Access*, vol. 7, pp. 12 742–12 754, 2019.

[13] Y. Yang, C. Chen, W. Zhang, X. Deng, P. Du, H. Yang, W.-D. Zhong, and L. Chen, "Secure and private NOMA VLC using OFDM with two-level chaotic encryption," *Opt. Express*, vol. 26, no. 26, pp. 34 031–34 042, Dec 2018.

[14] H. Chun, S. Rajbhandari, G. Faulkner, D. Tsonev, E. Xie, J. J. D. McKendry, E. Gu, M. D. Dawson, D. C. O'Brien, and H. Haas, "LED based wavelength division multiplexed 10 Gb/s visible light communications," *Journal of Lightwave Technology*, vol. 34, no. 13, pp. 3047–3052, 2016.

[15] L. Cui, Y. Tang, H. Jia, J. Luo, and B. Gnade, "Analysis of the multichannel WDM-VLC communication system," *Journal of Lightwave Technology*, vol. 34, no. 24, pp. 5627–5634, 2016.

[16] F. M. Wu, C. T. Lin, C. C. Wei, C. W. Chen, Z. Y. Chen, H. T. Huang, and S. Chi, "Performance comparison of OFDM signal and CAP signal over high capacity RGB-LED-based WDM visible light communication," *IEEE Photonics Journal*, vol. 5, no. 4, pp. 7 901 507–7 901 507, 2013.

[17] X. Li, Z. Ghassemlooy, S. Zvánovec, and P. A. Haigh, "A 40 Mb/s VLC system reusing an existing large LED panel in an indoor office environment," *Sensors*, vol. 21, no. 5, 2021.

[18] Q. Hu, X. Jin, W. Liu, D. Guo, M. Jin, and Z. Xu, "Comparison of interpolation-based sampling frequency offset compensation schemes for practical OFDM-VLC systems," *Opt. Express*, vol. 28, no. 2, pp. 2337–2348, Jan 2020.

[19] C.-H. Yeh, H.-Y. Chen, C.-W. Chow, and Y.-L. Liu, "Utilization of multi-band OFDM modulation to increase traffic rate of phosphor-LED wireless VLC," *Opt. Express*, vol. 23, no. 2, pp. 1133–1138, Jan 2015.

[20] D. Tsonev, S. Videv, and H. Haas, "Towards a 100 Gb/s visible light wireless access network," *Opt. Express*, vol. 23, no. 2, pp. 1627–1637, Jan 2015.

[21] J.-Y. Sung, C.-W. Chow, and C.-H. Yeh, "Is blue optical filter necessary in high speed phosphor-based white light LED visible light communications?" *Opt. Express*, vol. 22, no. 17, pp. 20 646–20 651, Aug 2014.

[22] H. Le Minh, D. O'Brien, G. Faulkner, L. Zeng, K. Lee, D. Jung, Y. Oh, and E. T. Won, "100-Mb/s NRZ visible light communications using a postequalized white LED," *IEEE Photonics Technology Letters*, vol. 21, no. 15, pp. 1063–1065, 2009.

[23] X. Li, Z. Ghassemlooy, S. Zvanovec, R. Perez-Jimenez, and P. A. Haigh, "Should analogue pre-equalisers be avoided in VLC systems?" *IEEE Photonics Journal*, vol. 12, no. 2, pp. 1–14, 2020.

[24] A. Tsiatmas, F. M. Willems, J.-P. M. Linnartz, S. Baggen, and J. W. Bergmans, "Joint illumination and visible-light communication systems: Data rates and extra power consumption," in *2015 IEEE International Conference on Communication Workshop (ICCW)*, 2015, pp. 1380–1386.

[25] A. Alexeev, J.-P. M. G. Linnartz, K. Arulandu, and X. Deng, "Characterization of dynamic distortion in LED light output for optical wireless communications," *Photon. Res.*, vol. 9, no. 6, pp. 916–928, Jun 2021.

[26] X. Li, Z. Ghassemlooy, S. Zvanovec, M. Zhang, and A. Burton, "Equivalent circuit model of high power LEDs for VLC systems," in *2019 2nd West Asian Colloquium on Optical Wireless Communications (WACOWC)*, 2019, pp. 90–95.

[27] X. Li, Z. Ghassemlooy, S. Zvanovec, and L. N. Alves, "An equivalent circuit model of a commercial LED with an ESD protection component for VLC," *IEEE Photonics Technology Letters*, vol. 33, no. 15, pp. 777–779, 2021.

[28] P.-C. Song, Z.-Y. Wu, X.-D. An, and J. Wang, "Energy efficiency analysis of light-emitting diodes with high modulation bandwidth," *IEEE Electron Device Letters*, vol. 42, no. 7, pp. 1025–1028, 2021.

[29] P. Salvador, J. Valls, J. L. Corral, V. Almenar, and M. J. Canet, "Linear response modeling of high luminous flux phosphor-coated white LEDs for VLC," *Journal of Lightwave Technology*, pp. 1–1, 2022.

[30] J. Armstrong, "OFDM for optical communications," *Journal of Lightwave Technology*, vol. 27, no. 3, pp. 189–204, 2009.

[31] D. Bykhovsky and S. Arnon, "An experimental comparison of different bit-and-power-allocation algorithms for DCO-OFDM," *Journal of Lightwave Technology*, vol. 32, no. 8, pp. 1559–1564, 2014.

[32] P. A. Haigh, A. Burton, K. Werfli, H. L. Minh, E. Bentley, P. Chvojka, W. O. Popoola, I. Papakonstantinou, and S. Zvanovec, "A multi-CAP visible-light communications system with 4.85-b/s/hz spectral efficiency," *IEEE Journal on Selected Areas in Communications*, vol. 33, no. 9, pp. 1771–1779, 2015.

[33] I.-T. S. Group, "ITU-T Rec. G.975.1 (02/2004) Forward error correction for high bit-rate DWDM submarine systems," *Standard*, pp. 1–58, 2005.

[34] R. Schmogrow, B. Nebendahl, M. Winter, A. Josten, D. Hillerkuss, S. Koenig, J. Meyer, M. Dreschmann, M. Huebner, C. Koos, J. Becker, W. Freude, and J. Leuthold, "Error vector magnitude as a performance measure for advanced modulation formats," *IEEE Photonics Technology Letters*, vol. 24, no. 1, pp. 61–63, 2012.

[35] D. Hughes-Hartogs, "Ensemble modem structure for imperfect transmission media," U.S. Patent 4 679 227A, 7 7, 1987.